Article

A Novel Positional Calibration Method for an Underwater Acoustic Beacon Array Based on the Equivalent Virtual Long Baseline Positioning Model

Ge Zhang [1], Guoxing Yi [1,*], Zhennan Wei [1,*], Yangguang Xie [2] and Ziyang Qi [3]

1 Space Control and Inertial Technology Research Center, Harbin Institute of Technology, Harbin 150001, China; zhangge@hit.edu.cn
2 Flight Automatic Control Research Institute, Aviation Industry Corporation of China, Xi'an 710065, China
3 Frontiers Science Center for Matter Behave in Space Environment, Harbin Institute of Technology, Harbin 150001, China
* Correspondence: ygx@hit.edu.cn (G.Y.); wzn@hit.edu.cn (Z.W.)

Abstract: The performance of long baseline (LBL) positioning systems is significantly impacted by the distribution and positional calibration accuracy of underwater acoustic beacon arrays. In previous calibration methods for beacon arrays based on autonomous underwater vehicle (AUV) platforms, the slant range information of each beacon was processed independently, and each beacon was calibrated one at a time. This approach not only decreases the calibration efficiency but also leaves the positional calibration accuracy of each beacon highly susceptible to the navigation trajectory of the AUV. To overcome these limitations, an equivalent virtual LBL (EVLBL) positioning model is introduced in this paper. This model operates by adjusting the positions of each beacon according to the dead reckoning increments computed during the AUV's reception of positioning signals, effectively forming a virtual beacon array. Consequently, the AUV is capable of mitigating LBL positioning errors that arise from its motion by simultaneously receiving positioning signals from all beacons. Additionally, an overall calibration method for beacon arrays based on particle swarm optimization (PSO) is proposed. In this approach, the minimization of the deviation between the EVLBL trajectory and the dead reckoning trajectory is set as the optimization objective, and the coordinates of each beacon are iteratively optimized. The simulation results demonstrate that the proposed EVLBL-based PSO algorithm (EVPSO) significantly enhanced the calibration efficiency and positional accuracy of the beacon array. Compared with conventional methods, the estimation error of the beacon positions was reduced from 6.40 m to within 1.00 m. After compensating for the beacon array positions, the positioning error of the LBL system decreased from approximately 5.00 m (with conventional methods) to around 1.00 m (with EVPSO), demonstrating the effectiveness of the proposed approach.

Keywords: underwater navigation; long baseline (LBL) acoustic positioning system; underwater acoustic beacon; calibration; particle swarm optimization (PSO)

1. Introduction

With the booming development of the marine economy, the exploitation and utilization of marine resources have increasingly garnered people's attention. Against this backdrop, the fields of underwater geological archaeology and geomorphological surveying [1], oil and gas exploration [2], underwater pipeline construction and maintenance [3,4], and underwater target rescue [5] have witnessed a growing demand for efficient and accurate underwater navigation technologies.

The long baseline (LBL) acoustic positioning system utilizes multiple acoustic beacons deployed underwater to calculate the position of vehicles by measuring the propagation time of acoustic signals from each beacon to the target [6]. Owing to its exceptional

positioning accuracy, stability, and scalability, an LBL plays an increasingly crucial role in underwater navigation applications [7,8]. Despite the numerous advantages of LBL positioning technology, it still faces several challenges in engineering applications. Among them, the deployment and positional calibration of underwater beacons have the most significant impact on the LBL positioning accuracy [9,10].

Floating LBLs have been widely used in underwater positioning practice due to their ability to accurately obtain global positioning system (GPS) information through buoys [11]. However, the positions of the buoys are susceptible to the water current, making them unsuitable for providing stable positioning services to underwater targets for extended periods. Furthermore, in scenarios requiring high concealment, the use of buoys is not advisable.

Underwater beacons are typically released from a workboat on the surface and subsequently come to anchor on the seabed at an unknown location. Due to the influence of water currents and other factors, there is often a significant horizontal deviation between the anchoring position of the beacon and its release position. Therefore, it is necessary to calibrate its actual position. During the conventional calibration process, the workboat sails on the water surface above the beacon release position, following a preset trajectory with the release position as the center. The vessel's GPS position and slant range data are recorded, and then the estimated position of each beacon is obtained through a least squares calculation based on geometric relationships [12]. This method necessitates considerable time to calibrate each beacon, thus limiting the operational efficiency. Furthermore, the method may fail to effectively mitigate ranging errors that arise from variations in sound speed, thereby compromising the desired accuracy. To enhance the calibration accuracy, Zhang et al. proposed underwater transponder calibration methods based on a Gauss–Newton iteration algorithm [13] and adaptive fault-tolerant Kalman filters [14]. Similarly, a calibration method based on M-estimation is proposed in reference [15] and was verified for subsea wellhead positioning. Building on this, a calibration method that integrates the interactive multiple model with the unscented Kalman filter is proposed in reference [16]. This method enables the efficient calibration of beacon positioning errors while also accounting for installation errors in the strapdown inertial navigation system (SINS) and the transceiver of the ultra-short baseline (USBL) acoustic positioning system. Although the aforementioned methods have significantly improved calibration accuracy compared with conventional approaches, the use of a USBL for beacon calibration in large-scale applications still inevitably leads to insufficient calibration accuracy due to limitations in the ranging precision. Consequently, the utilization of an LBL for beacon calibration continues to be the prevalent approach in current practices. Distinguishing from other methods, a perpendicular intersection-based approach that utilizes analytic geometry and least squares methods to achieve beacon calibration is proposed in reference [17]. A relatively comprehensive error model for beacon calibration using an LBL that innovatively incorporates beacon position errors into the state variables is presented in reference [18]. This approach enables the simultaneous estimation of the target position while calibrating the beacon positions. Xu et al. dedicated their efforts to exploring ways to improve the calibration accuracy and efficiency of underwater beacons without the support of depth sensors. They successively proposed calibration methods based on local area segmentation and an improved salp swarm algorithm [19,20], achieving high-precision depth estimation. In reference [21], a beacon calibration method based on extended competitive particle swarm optimization is proposed. While certain algorithms demonstrated success in enhancing the calibration accuracy of underwater acoustic beacons, they still adhere to the conventional calibration mode, requiring the workboat to navigate a fixed trajectory. Consequently, there remains considerable potential for further optimizing and elevating the calibration efficiency. Addressing this issue, Ji et al. proposed a novel method for beacon calibration using an autonomous underwater vehicle (AUV) [22,23]. This method integrates the slant range information from the beacons with a SINS, leveraging the extended Kalman filter technique to simultaneously localize the AUV and calibrate the beacon positions. On this

basis, factor graph optimization was applied to underwater acoustic beacon calibration in reference [24]. In this method, a Doppler velocity log (DVL), a SINS, a depth gauge, and beacons were abstracted as factors within the optimization framework, enabling simultaneous AUV localization and acoustic beacon estimation. Although the efficiency and accuracy of the aforementioned methods have improved, they still essentially belong to the method of calibrating each beacon's position individually, which inevitably results in the calibration accuracy of beacon positions being affected by their distance from the AUV. In other words, in a beacon array, the position calibration accuracy of beacons is generally better for those that are closer to the AUV's navigation trajectory and lower for those that are farther from it. In addition, the impact of the LBL positioning error caused by the movement of the AUV on the beacon position calibration was not taken into account by previous methods.

In this study, the equivalent virtual LBL (EVLBL) positioning method is proposed to address the issue of inaccurate position estimation caused by AUV motion during the LBL position calculation process. In this method, the position of each beacon is virtually translated according to the dead reckoning increment after its positioning signal reaches the AUV, and finally forms an equivalent virtual beacon array when calculating the LBL position. Through this method, the slant range error of each beacon caused by the movement of the AUV is eliminated, thereby effectively improving the positioning accuracy of the LBL system. On this basis, an overall calibration method for underwater acoustic beacon arrays is proposed. Distinct from previous related studies that process the slant range data of each beacon individually and calibrate the beacons one by one, this method treats all beacons as a unified entity and abstracts them into a state variable. The EVLBL-based trajectory derived from this state variable is then compared with the dead reckoning trajectory. With the aim of minimizing the deviation between the two trajectories, the particle swarm optimization (PSO) algorithm is employed for iterative optimization. Once the deviation reaches its minimum value, the optimal estimates of the positions of each beacon can be obtained.

The structure of this paper is organized as follows. In Section 2, the LBL positioning error model is established, and the positioning errors that arise from AUV motion are analyzed. Based on this, the EVLBL positioning model is constructed. In Section 3, the underwater acoustic beacon array calibration method based on PSO is explained, along with its optimization using the EVLBL positioning model. The simulation test in Section 4 verifies the effectiveness and accuracy of the proposed method. The conclusions are presented in Section 5.

2. Model of EVLBL

In comparison with underwater acoustic transponders, the employment of periodic sound source beacons for passive acoustic positioning offers notable improvements in both the concealment and safety of AUVs. Furthermore, by eliminating the requirement for transmitting transducer configurations, this approach effectively manages the costs, providing a more economically viable and efficient solution for marine exploration and positioning applications [25]. Despite these advantages, however, the adoption of this method also necessitates the consideration of LBL positioning errors induced by AUV motion.

2.1. Analysis of LBL Positioning Errors Caused by AUV Motion

Figure 1 depicts a schematic diagram illustrating the LBL positioning process of AUVs based on an acoustic beacon array, which consists of three synchronized sound source beacons. Each beacon broadcasts positioning information to the surrounding area at predetermined time intervals T_0. This positioning information should include critical data, such as the unique identifier of the beacon, the precise time of signal transmission, and the current position of the beacon. In a certain LBL positioning cycle, all beacons synchronously broadcast positioning information at time t_0. After the signals propagate through the water, they are captured by the AUV at positions P_{A1}, P_{A2}, and P_{A3} at t_1, t_2, and t_3, respectively. As the AUV remains stationary during this period, it follows that $P_{A1} = P_{A2} = P_{A3}$.
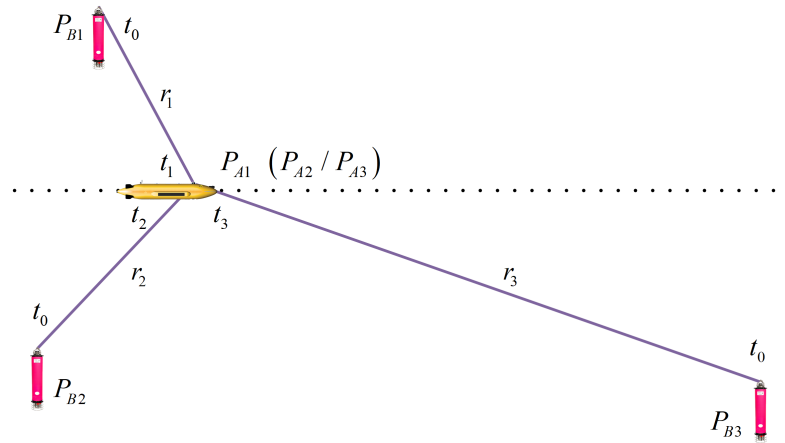
Figure 1. Schematic diagram of the LBL positioning process employing a sound source beacon array.

The slant range between the AUV and beacon k can be expressed as

$$r_k = (t_k - t_0)v_s \tag{1}$$

where $k = 1, 2, 3$ represents the beacon index; r_k denotes the slant range from beacon k to the AUV; and v_s represents the average speed of sound signal propagation in water, as measured by a sound velocity profiler.

To facilitate the problem exposition, this paper assumes $t_1 < t_2 < t_3$. Thus, upon the reception of positioning signals from all the beacons by the AUV, the current position can be determined using the trilateration model. Considering that AUVs are commonly equipped with depth sensors for acquiring precise vertical position data, this study primarily concentrated on estimating the horizontal position. The specific calculation formula is outlined as follows:

$$\hat{P}_{A3} = A^{-1}B \tag{2}$$

$$A = \begin{bmatrix} x_{B1} - x_{B3} & y_{B1} - y_{B3} \\ x_{B2} - x_{B3} & y_{B2} - y_{B3} \end{bmatrix} \tag{3}$$

$$B = \begin{bmatrix} \frac{1}{2}(s_1 - s_3) - (z_{B1} - z_{B3})\hat{z}_{A3} \\ \frac{1}{2}(s_2 - s_3) - (z_{B2} - z_{B3})\hat{z}_{A3} \end{bmatrix} \tag{4}$$

$$s_k = (x_{Bk})^2 + (y_{Bk})^2 + (z_{Bk})^2 - (r_k)^2 \tag{5}$$

where $\hat{P}_{A3} = [\hat{x}_{A3}, \hat{y}_{A3}]^{\mathrm{T}}$ represents the estimation value of the horizontal position of the AUV by the LBL system at t_3, $P_{Bk} = [x_{Bk}, y_{Bk}, z_{Bk}]^{\mathrm{T}}$ represents the position coordinates of beacon k in the Cartesian coordinate system, and $\hat{z}_{A3}$ represents the depth measurement of the AUV at t_3.

When the AUV moves during the positioning process, as depicted in Figure 2, the reception positions of the positioning signals from each beacon (P_{A1} and P_{A2}) do not coincide with the LBL-calculated position (P_{A3}). Consequently, there exists a deviation between the actual slant ranges r'_k and the calculated slant ranges r_k based on Equation (1). If the position estimation of the AUV is still based on Equations (2)–(5), there will inevitably be positioning errors.

To simplify this issue, it is considered that the AUV moves solely in the horizontal direction, i.e., constant depth navigation is conducted. Taking beacon 1 as an example, the calculation of the actual slant range r'_k between each beacon and the AUV at P_{A3} is as follows:

$$r'_1 = \|P_{B1} - P_{A3}\| = \|P_{B1} - (P_{A1} + \Delta P_{A13})\| \tag{6}$$

where $\|\|$ denotes the operation of calculating the Euclidean distance. ΔP_{A13} represents the dead reckoning positional increment of the AUV from times t_1 to t_3, which can be expressed as follows:

$$\Delta P_{A13} = \int_{t_1}^{t_3} V_A(t)dt \tag{7}$$

where $V_A(t) = \left[v_{Ax}(t), v_{Ay}(t)\right]^{\mathrm{T}}$ represents the velocities of the AUV along the x-axis and y-axis at time t. Then, r'_1 can be further expressed as

$$(r'_1)^2 = (r_1)^2 + (\Delta x_{A13})^2 + [\Delta y_{A13}]^2 + 2\Delta x_{A13}(x_{B1} - x_{A1}) + 2\Delta y_{A13}(y_{B1} - y_{A1}) \tag{8}$$

$$\Delta x_{A13} = \int_{t_1}^{t_3} v_{Ax}(t)dt \tag{9}$$

$$\Delta y_{A13} = \int_{t_1}^{t_3} v_{Ay}(t)dt \tag{10}$$
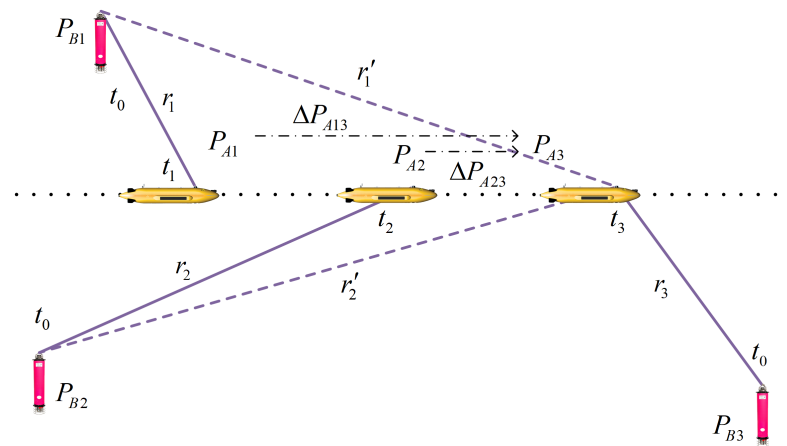

Figure 2. Schematic diagram of LBL positioning process under AUV motion.

The actual slant range r'_2 of beacon 2 can be similarly obtained based on Equation (8). Using $\hat{P}'_{A3} = [\hat{x}'_{A3}, \hat{y}'_{A3}]$ to represent the estimated position of the AUV based on the actual slant ranges for LBL calculation, the process of the trilateration calculation can be expressed as

$$\hat{P}'_{A3} = \begin{bmatrix} x_{B1} - x_{B3} & y_{B1} - y_{B3} \\ x_{B2} - x_{B3} & y_{B2} - y_{B3} \end{bmatrix}^{-1} \begin{bmatrix} \frac{1}{2}(s'_1 - s'_3) - (z_{B1} - z_{B3})\hat{z}_{A3} \\ \frac{1}{2}(s'_2 - s'_3) - (z_{B2} - z_{B3})\hat{z}_{A3} \end{bmatrix} \tag{11}$$

$$s'_k = (x_{Bk})^2 + (y_{Bk})^2 + (z_{Bk})^2 - (r'_k)^2 \tag{12}$$

Combining the above equations, the positioning error of the AUV can ultimately be expressed as

$$\begin{aligned} \delta P_{A3} &= \hat{P}'_{A3} - \hat{P}_{A3} \\ &= -\frac{1}{2}A^{-1}\begin{bmatrix} (\Delta x_{A13})^2 + [\Delta y_{A13}]^2 + 2\Delta x_{A13}(x_{B1} - x_{A1}) + 2\Delta y_{A13}(y_{B1} - y_{A1}) \\ (\Delta x_{A23})^2 + [\Delta y_{A23}]^2 + 2\Delta x_{A23}(x_{B2} - x_{A2}) + 2\Delta y_{A23}(y_{B2} - y_{A2}) \end{bmatrix} \end{aligned} \tag{13}$$

As depicted in Equations (8) and (13), the positioning error induced by the AUV motion involves multiple interrelated variables, primarily including the AUV's velocity and trajectory and the configuration of the beacon array. These variables are interrelated and difficult to separate for quantitative analysis. Only a rough description can be provided based on the equations: the further the deviation of the AUV's trajectory from the center of

the beacon array and the faster the AUV's velocity, the larger the positioning error of the LBL will be.

2.2. EVLBL Positioning Model Based on Dead Reckoning

Due to the high complexity and decoupling difficulty of the LBL positioning error model described in Equation (13), compensating for these errors in practical applications presents significant challenges. Therefore, conventional methods that rely on compensating for positioning errors based on range information were not utilized in this study. Instead, an innovative strategy that involves equivalent translation acoustic beacons is proposed. This approach entails constructing a virtual beacon array for the LBL calculation, thereby effectively eliminating the positioning error.

When directly using r_k as the slant range from beacon k to the AUV for the LBL position calculation, this implies that the corresponding beacon position moves from P_{BK} to $\tilde{P}_{Bk} = [\tilde{x}_{Bk}, \tilde{y}_{Bk}, \tilde{z}_{Bk}]^{\mathrm{T}}$. This results in the construction of a virtual beacon array composed of one real beacon located at P_{B3} and two virtual beacons located at $\tilde{P}_{B1}$ and $\tilde{P}_{B2}$ at time t_3, as shown in Figure 3. Taking beacon 1 as an example, the equivalent virtual translation can be represented as

$$\tilde{P}_{B1} = P_{B1} + \Delta P_{B1} \tag{14}$$

where P_{B1} is the actual position of beacon 1. $\tilde{P}_{B1}$ represents the position of beacon 1 in the virtual beacon array after the equivalent translation. ΔP_{B1} is the position translation of beacon 1, which is equal to the dead reckoning positional increment ΔP_{A13} of the AUV from times t_1 to t_3. In summary, the position of beacon 1 in the virtual beacon array can be represented as

$$\tilde{P}_{B1} = P_{B1} + \int_{t_1}^{t_3} C_b^n(t) \cdot V^b(t) dt \tag{15}$$

where $V^b(t)$ represents the velocity of the AUV in the body coordinate system at time t, as measured by the DVL. $C_b^n(t)$ represents the direction cosine matrix at time t, as computed from attitude angles measured by the compass.
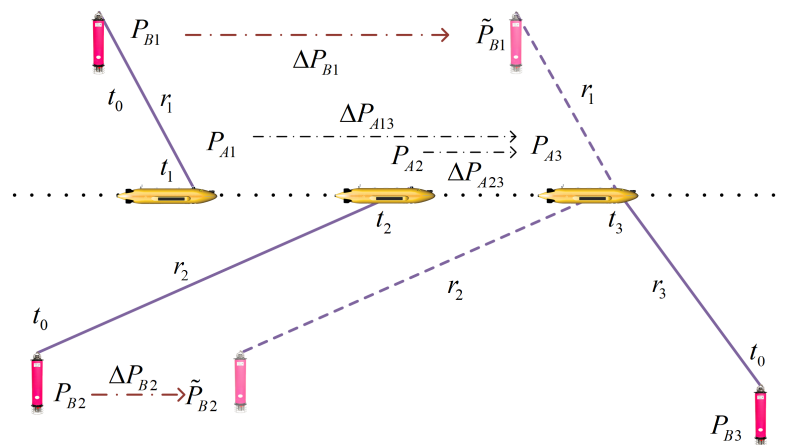

Figure 3. Schematic diagram of EVLBL.

The position of beacon 2 in the virtual beacon array can be similarly obtained according to Equation (15). The calculation process for the AUV position based on the EVLBL positioning model can be expressed as follows:

$$P_{EVLBL} = \begin{bmatrix} \tilde{x}_{B1} - x_{B3} & \tilde{y}_{B1} - y_{B3} \\ \tilde{x}_{B2} - x_{B3} & \tilde{y}_{B2} - y_{B3} \end{bmatrix}^{-1} \begin{bmatrix} \frac{1}{2}(\tilde{s}_1 - s_3) - (\tilde{z}_{B1} - z_{B3})\hat{z}_{A3} \\ \frac{1}{2}(\tilde{s}_2 - s_3) - (\tilde{z}_{B2} - z_{B3})\hat{z}_{A3} \end{bmatrix} \tag{16}$$

$$\tilde{s}_k = (\tilde{x}_{Bk})^2 + (\tilde{y}_{Bk})^2 + (\tilde{z}_{Bk})^2 - (r_k)^2 \tag{17}$$

3. Overall Calibration Method for Acoustic Beacon Array

3.1. Calibration Method Based on Trajectory Deviations

Figure 4 illustrates the schematic diagram of the overall calibration method for the beacon array based on the extent of the overlap between the dead reckoning trajectory and the LBL trajectory. The method primarily consists of three parts: dead reckoning trajectory calculation, LBL trajectory calculation, and beacon position optimization iteration. Within the dead reckoning module, the position increment of the AUV is computed based on measurements from the compass and DVL. Subsequently, a trajectory T_{DR} is generated based on the known initial position, as illustrated in Equation (18). Within the LBL trajectory calculation module, the LBL position of the AUV is computed based on the beacon array coordinates and measurements of the slant range data. Subsequently, the trajectory T_{LBL} is generated as depicted in Equation (19). Within the beacon position optimization iteration module, the extent of overlap between T_{DR} and T_{LBL} is first computed, and minimizing this value is set as the optimization objective. Subsequently, the coordinates of each beacon are iteratively adjusted until the optimal solution is achieved.
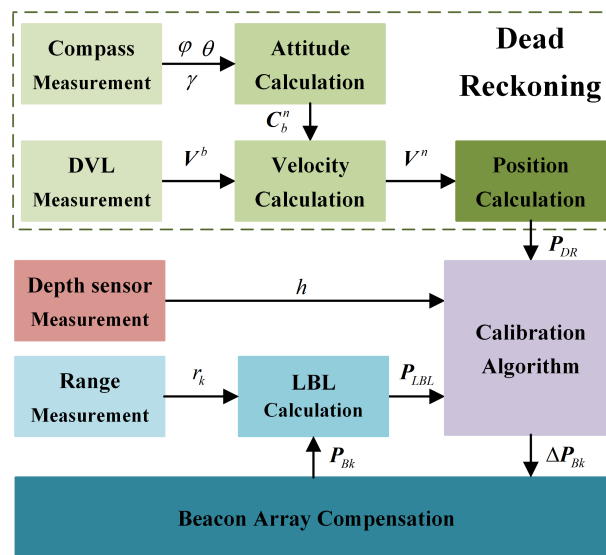

Figure 4. Block diagram of the beacon array calibration method based on the extent of the overlap between the dead reckoning trajectory and the LBL trajectory.

$$T_{DR} = \left[P_{DR}(t_{s1}), P_{DR}(t_{s2}), \cdots , P_{DR}\left(t_{sj}\right), \cdots , P_{DR}(t_{sN}) \right] \tag{18}$$

$$T_{LBL} = \left[P_{LBL}(t_{s1}), P_{LBL}(t_{s2}), \cdots , P_{LBL}\left(t_{sj}\right), \cdots , P_{LBL}(t_{sN}) \right] \tag{19}$$

where $j = 1, 2, \cdots , N$ denotes the index of the positioning signals emitted by each beacon in the array toward the AUV at a fixed interval starting from the moment the calibration algorithm is executed; N represents the total number of positioning signals emitted by the beacon array throughout the entire calibration process; t_{sj} represents the moment when the AUV fully receives the j-th set of positioning signals and conducted the trilateration calculation; and $P_{LBL}\left(t_{sj}\right)$ and $P_{DR}\left(t_{sj}\right)$, respectively, represent the LBL-calculated position and the dead reckoning position of the AUV at time t_{sj}, as obtained from Equations (16) and (20).

$$P_{DR}\left(t_{sj}\right) = P_{DR}\left(t_{s(j-1)}\right) + \int_{t_{s(j-1)}}^{t_{sj}} C_b^n(t) \cdot V^b(t) dt \tag{20}$$

The error of T_{LBL} relative to the reference trajectory T_{DR} is used as the objective function, as shown in Equation (22).

$$\varepsilon(j) = \begin{bmatrix} \varepsilon_x(j) & \varepsilon_y(j) \end{bmatrix}^T = P_{LBL}(t_{sj}) - P_{DR}(t_{sj}) \tag{21}$$

$$f(x) = \frac{1}{N} \cdot \sum_{j=1}^{N} \sqrt{[\varepsilon_x(j)]^2 + [\varepsilon_y(j)]^2} \tag{22}$$

where $\varepsilon(j)$ represents the trajectory error; $\varepsilon_x(j)$ and $\varepsilon_y(j)$ represent the components of $\varepsilon(j)$ on the x-axis and y-axis, respectively; and x represents the parameters to be optimized.

By utilizing the coordinates of each beacon in the array as optimization parameters, denoted as x, and by minimizing the objective function $f(x)$, the overall calibration of the beacon array can be successfully achieved through the application of an appropriate parameter optimization algorithm.

3.2. Implementation of Beacon Calibration Method Based on PSO

PSO is a population-based stochastic optimization technique inspired by collective behaviors observed in nature, such as the cooperative foraging patterns seen in insects, herds, flocks of birds, and schools of fish. In PSO, each particle represents a potential solution and independently explores the search space to find the best individual solution. Meanwhile, the entire swarm of particles operates collectively, iteratively selecting the global best solution. During the search process, particles dynamically adjust their search direction and step size based on their individual and global best solutions. This dynamic adjustment mechanism enables PSO to rapidly converge toward the optimal solution and effectively avoid local optima.

Taking the coordinates of each beacon in the array as parameters to be optimized, a particle swarm is generated, with the minimization of the fitness value calculated by the objective function serving as the optimization criterion. As the particle swarm continuously iterates within the PSO optimizer based on the EVLBL positioning model, the overall calibration of the beacon array can be achieved.

The coordinates of the beacon array are abstracted as a particle position, which is represented as follows:

$$\begin{aligned} x_i(t) &= [x_{i1}(t), x_{i2}(t), x_{i3}(t), x_{i4}(t), x_{i5}(t), x_{i6}(t)] \\ &= [x_{B1}(t), y_{B1}(t), x_{B2}(t), y_{B2}(t), x_{B3}(t), y_{B3}(t)] \end{aligned} \tag{23}$$

where $i = 1, 2, \cdots, Np$ represents the index of each particle, with Np denoting the total number of particles in the swarm; similarly, $t = 1, 2, \cdots, T_{\max}$ indicates the iteration number, where $T_{\max}$ is the maximum number of iterations in the PSO optimization process; and $x_i(t)$ denotes the position of particle i in the t-th iteration, represented as a six-dimensional vector indicating the x and y coordinates of each beacon in the Cartesian coordinate system. The update rule governing the evolution of these positions is outlined in Equation (24).

$$x_i(t+1) = x_i(t) + t_p v_i(t+1) \tag{24}$$

where $v_i(t+1)$ represents the velocity of particle i in the $(t+1)$-th iteration, which quantifies the changing rate of the particle's position. Similar to the particle position, it is also a six-dimensional vector. The update rule for the velocity is given in Equation (25). t_p represents the time step, which is generally defaulted to a unit time step, i.e., its value is set to 1 in this context.

$$v_i(t+1) = \omega_p v_i(t) + c_1 r_1 \left[p_i^{pb} - x_i(t) \right] + c_2 r_2 \left[p^{gb} - x_i(t) \right] \tag{25}$$

where ω_p represents the inertia weight, reflecting the degree to which the particle velocity update is influenced by the magnitude and direction of the particle velocity in the previous iteration; c_1 is the cognitive coefficient, indicating the extent to which the particle velocity update is influenced by its historical best position p_i^{pb}; c_2 is the social coefficient, reflecting the extent to which the particle velocity update is influenced by the global best position p^{gb} of the swarm; and r_1 and r_2 are random numbers between 0 and 1.

The personal best value f_i^{pb} is the minimum fitness value of particle i in the current iteration process, and its corresponding particle position is p_i^{pb}. Similarly, the global best value f^{gb} is the minimum value of all the particles' personal best values in the swarm during the current iteration process, and its corresponding particle position is p^{gb}.

During the iterative process of PSO, the personal best positions of particles within the swarm are continuously updated as the fitness values are computed. Concurrently, the global best position of the swarm is also updated. All particles in the swarm continuously move in the direction of the lowest fitness value with the assistance of their individual cognition and group information. Additionally, the positions of all beacons gradually iterate in the direction of the optimal estimate. When the particle swarm optimizer reaches the stopping condition, the beacon array coordinates ultimately achieve the optimal estimation. The overall calibration algorithm process of the beacon array based on PSO is shown in Algorithm 1.

Algorithm 1 Calibration method of acoustic beacon array based on PSO.

    Input: Coordinate transformation matrix based on compass measurement data C_b^n. Measurement data from DVL V^b. Measurement data from beacons R_k and measurement data from depth sensor h.
    Output: Estimated value of beacon array location $[\hat{x}_{B1}, \hat{y}_{B1}, \hat{x}_{B2}, \hat{y}_{B2}, \hat{x}_{B3}, \hat{y}_{B3}]$.
1: Initialize the particle's position with a uniformly distributed random vector, and initialize each particle's velocity at 0.
2: Calculate the fitness values of the particles; then, determine f^{gb}, p^{gb}, and p_i^{pb}.
3: Calculate the dead reckoning trajectory T_{DR} of the AUV based on C_b^n and V^b.
4: **while** stop condition not reached **do**
5:     **for** each particle i **do**
6:         Calculate the position of the virtual beacon array according to Equation (15).
7:         Calculate the fitness value $f(x_i)$ according to Equation (22);
8:         **if** $f(x_i) < f_i^{pb}$ **then**
9:             Update the personal best value f_i^{pb} and the best known position p_i^{pb}.
10:         **end if**
11:     **end for**
12:     **if** $\min\left[f_1^{pb} \; f_2^{pb} \; \cdots \; f_{Np}^{pb} \right] \leq f^{gb}$ **then**
13:         Update the global best value f^{gb} and the best known position p^{gb} of the swarm.
14:     **end if**
15:     **if** stop condition reached **then**
16:         Stop the PSO iteration.
17:     **end if**
18:     Update the particles' velocities according to Equation (25).
19:     Update the particles' positions according to Equation (24).
20: **end while**
21: Calculate the beacon array location: $[\hat{x}_{B1}, \hat{y}_{B1}, \hat{x}_{B2}, \hat{y}_{B2}, \hat{x}_{B3}, \hat{y}_{B3}] = p^{gb}$.

It should be emphasized that the stopping criteria of the algorithm and parameters involved, such as the inertia weight, cognitive coefficient, and social coefficient, need to be adjusted according to specific circumstances. In the simulation experiments in this study, we chose to stop the iterations after 200 runs. The value of ω_p was set to 0.9, while the values of c_1 and c_2 were both set to 2.

4. Simulation

4.1. Conditions for the Simulation

To validate the effectiveness and accuracy of the underwater beacon array position estimation method based on the EVLBL positioning model, a simulation experiment was conducted under the following conditions:

1. The distribution of the underwater acoustic beacons within the array is depicted in Figure 5. The green stars represent the release positions of the beacons, indicating the coordinates where the beacons were deployed on the water surface. The blue stars indicate the anchored positions of the beacons, representing their actual locations on the seabed after being influenced by factors such as water currents. The specific positions are detailed in Table 1.

2. The simulated trajectory of the AUV is illustrated in Figure 5. The trajectory began from $(203.42, 946.99, -749.99)$ and then underwent a continuous spiral descent motion lasting for 1200 s at a constant speed. Throughout the entire process, the AUV completed a clockwise rotation of 360.0 degrees to simulate the motion state in a real ocean environment.

3. The AUV travelled in a clockwise direction, with the heading angle increasing from 30.0 degrees at a constant angular velocity, completing one full rotation. The pitch angle decreased uniformly from 0 to around -1.5 degrees during the spiral descent process and remained constant, uniformly returning to 0 before the end of the trajectory. The roll angle fluctuated near 0 throughout. The specific attitude angle data are shown in Figure 6a.

4. The forward velocity v_y^b of the AUV maintained a constant speed of 4.00 m/s, while the right velocity v_x^b and upward velocity v_z^b remained near 0. Specific data are shown in Figure 6b.

5. The measurement noise for each attitude angle of the compass was white noise with a standard deviation of $0.30°$.

6. The measurement noise for the velocity in each direction of the DVL was white noise with a standard deviation of 0.01 m/s.

7. The ranging error of the underwater acoustic beacon was specified as 0.1% of the slant range, which was compounded with white noise with a standard deviation of 0.1 m.
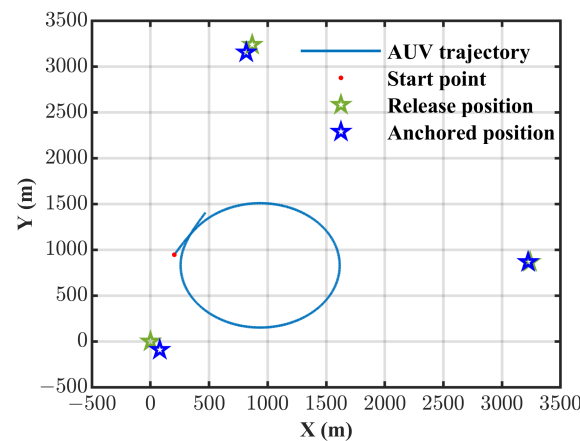

Figure 5. Schematic diagram of the AUV simulation trajectory and beacon array location.

Table 1. Distribution of the beacon array in the simulation test.

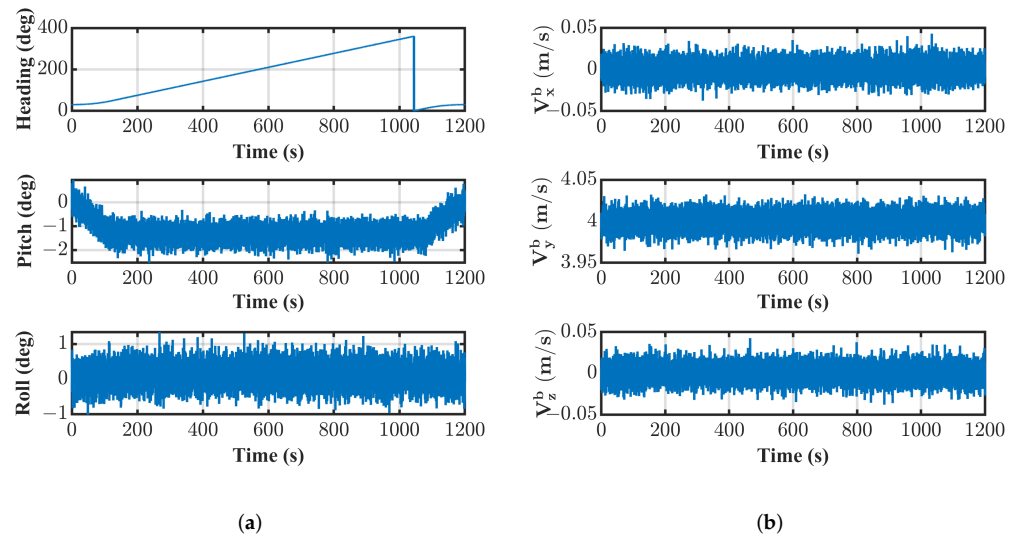| Position	Beacon 1	Beacon 2	Beacon 3
Release point	(0.00, 0.00, 0.00)	(3239.81, 868.11, 0.00)	(868.11, 3239.81, 0.00)
Anchored point	(79.36, −91.52, −1018.97)	(3223.05, 867.79, −1000.26)	(817.26, 3156.09, −1008.66)

Figure 6. Measurement data in simulation test: (**a**) attitude information from compass; (**b**) velocity information data from DVL.

4.2. Results and Discussion of the Simulation

Drawing upon the aforementioned simulated data, comprehensive simulation tests were conducted on the proposed underwater beacon array positional calibration algorithm based on EVLBL and PSO (hereafter referred to as EVPSO). In addition, to demonstrate the effectiveness and advantages of the EVLBL positioning model, comparative simulation experiments were devised against the PSO algorithm employing a conventional LBL positioning model (hereafter referred to as PSO). Compared with the EVPSO algorithm, the standard PSO algorithm did not perform step 6 as described in Algorithm 1, which used the actual coordinates of the beacon array rather than virtual coordinates for the trilateration calculation. However, both methodologies adhered to the principle of iteratively optimizing the beacon array coordinates as a whole. Furthermore, to validate the effectiveness and advantages of the iterative optimization approach with respect to the beacon array as a whole, comparative simulation experiments were designed with the conventional approach based on the least squares algorithm, which separately processed the range data of each beacon and completed the calibration one by one (hereinafter referred to as LS). Table 2 provides the calibration results of these algorithms for the beacon array coordinates and their errors from the given values.

Table 2. Estimation results and errors of beacon array positions in simulation test.

Algorithm	$x_{B1}/\Delta x_{B1}$ (m)	$y_{B1}/\Delta y_{B1}$ (m)	$x_{B2}/\Delta x_{B2}$ (m)	$y_{B2}/\Delta y_{B2}$ (m)	$x_{B3}/\Delta x_{B3}$ (m)	$y_{B3}/\Delta y_{B3}$ (m)
Setpoint	79.36/0.00	−91.52/0.00	3223.05/0.00	867.79/−0.00	817.22/0.00	3156.09/0.00
LS	80.01/0.66	−91.43/0.09	3216.65/−6.40	867.77/−0.02	820.15/2.93	3156.98/0.89
PSO	76.52/−2.84	−89.32/2.20	3223.49/0.45	870.29/2.50	813.60/−3.61	3156.09/0.01
EVPSO	79.66/0.30	−92.22/−0.71	3223.42/0.38	866.94/−0.86	816.88/−0.34	3156.29/0.20

According to the data in this table, LS exhibited excellent accuracy in estimating the position of beacon 1, with the error within 1.00 m. However, for the estimation of beacon 2, the error significantly increased, reaching over 6.00 m. Similarly, the estimation error for beacon 3 also exceeded 2.00 m. This primarily stemmed from the fact that the LS algorithm employed a sequential calibration-data-processing approach, resulting in a higher calibration accuracy for beacons closer to the AUV trajectory due to smaller slant range errors. Conversely, beacons further away from the AUV trajectory suffered from larger slant range errors, leading to a relatively lower calibration accuracy.

In contrast, the PSO algorithm performed an overall calibration by utilizing the trajectory data generated from the LBL positioning of the AUV using the beacon array, thoroughly accounting for the effects of the slant range errors for each beacon. Therefore, its estimation results exhibit a more balanced trend, with the positioning error for all three beacons stabilized at around 3.00 m, demonstrating a certain level of stability. Nevertheless, there is still room for improvement in the calibration accuracy of the PSO algorithm. This is primarily due to the inconsistency in the reception timing of beacon signals in the conventional LBL positioning model when the AUV trajectory deviated from the center of the beacon array. This inconsistency led to an increase in the slant range errors of the beacons, thereby affecting the calibration accuracy. By compensating for this error through the EVLBL positioning model proposed in this paper, EVPSO achieved a significant improvement in calibration accuracy for the three beacons, with the calibration errors reduced to within 1.00 m.

Figure 7 illustrates the iteration curves for estimating the coordinates of beacons using the PSO and EVPSO algorithms. Specifically, Figure 7a presents the iteration curve of the fitness value, which not only reflects the iteration speed of the algorithm but also, to some extent, indicates the final calibration accuracy. Through comparative analysis, it is evident that EVPSO exhibited a faster convergence rate compared with PSO, with a lower convergence value (1.75 vs. 1.93). This advantage is primarily attributed to the effective compensation of slant range errors by the EVPSO algorithm. Figure 7b–d present the iteration curves of the x- and y-coordinate estimation values for beacon 1 to beacon 3, respectively. From these curves, it can be observed that EVPSO not only had a faster convergence speed compared with PSO but also that its final convergence value was closer to the given value, further validating the superiority of the EVPSO algorithm in the beacon array coordinate estimation.

After compensating for the beacon array position estimation results of the LS, PSO, and EVPSO algorithms, Figure 8 clearly illustrates the comparison of the LBL trajectories before and after calibration. Before calibration, the LBL trajectories gradually deviated from the true trajectory over time, exhibiting significant errors. However, after calibration with the LS, PSO, and EVPSO algorithms, all LBL trajectories showed significant improvement, closely aligning with the true trajectory and effectively reducing the positioning errors. Notably, the LBL trajectory calibrated by the EVPSO algorithm was even closer to the true trajectory compared with the other two methods, further demonstrating the higher accuracy and superiority of the EVPSO algorithm in beacon array calibration.

After calibration with the LS, PSO, and EVPSO algorithms, the positioning errors of the LBL trajectory compared with the true trajectory in the x- and y-directions are illustrated in Figure 9. The root-mean-square error (RMSE) of the LBL position error after compensation by each calibration method is presented in Table 3. From the figures and tables, it can be observed that the LBL position error after the LS calibration was significantly larger than that of the other two algorithms, indicating a larger deviation. In comparison, the LBL position error after the EVPSO calibration was slightly smaller than the result of PSO, demonstrating a higher calibration accuracy and stability.

Table 3. RMSE of LBL after beacon array calibration.

Algorithm	P_X (m)	P_Y (m)
Uncalibrated	17.81	67.83
LS	5.71	2.61
PSO	1.65	1.46
EVPSO	1.14	1.04

P_X and P_Y represent the components of the LBL positioning error in the x-axis and y-axis directions, respectively.
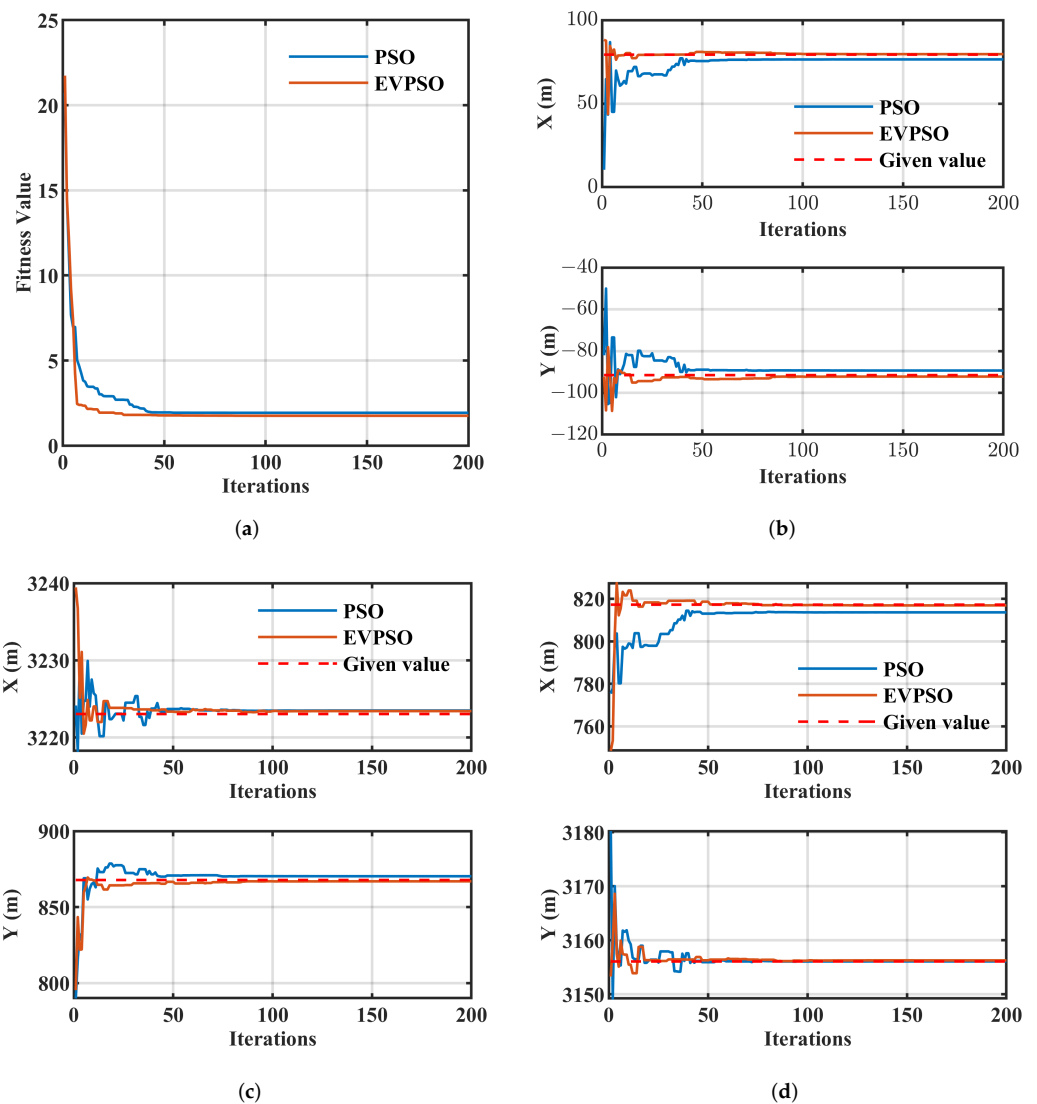
Figure 7. Iteration curves of beacon array position estimation based on PSO and EVPSO in simulation tests: (**a**) fitness value; (**b**) estimated position of beacon 1; (**c**) estimated position of beacon 2; (**d**) estimated position of beacon 3.
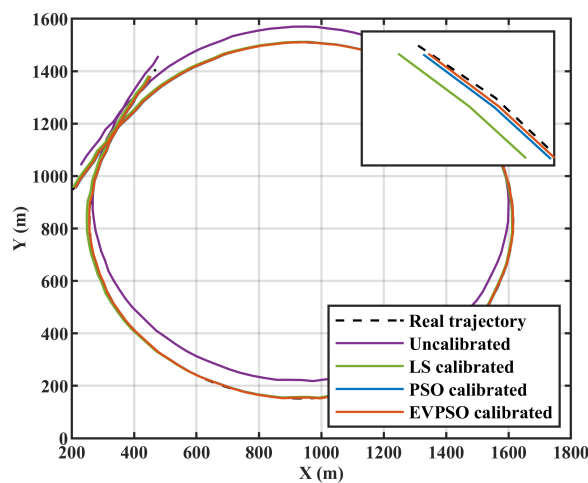

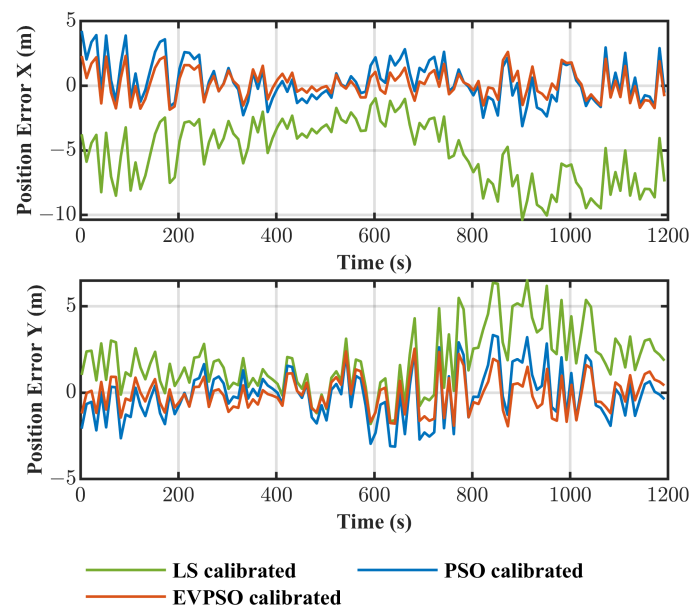**Figure 8.** Comparison of LBL trajectories before and after beacon array calibration.

Figure 9. Positioning error of LBL after beacon array calibration.

5. Conclusions

In this paper, an overall calibration method for underwater beacon arrays based on the EVLBL positioning model is proposed. First, a thorough analysis was conducted on the position errors in LBL calculations arising from time-synchronized acoustic source beacon arrays. Based on this analysis, the EVLBL positioning model was introduced, which incorporated the equivalent translation of beacons through the dead reckoning of an AUV. Building upon this, a beacon array coordinate parameter optimization search method is further proposed, with the objective of minimizing the discrepancy between the dead reckoning trajectory and the LBL trajectory. Through simulation verification using the PSO algorithm, it was demonstrated that this method is not only effective and feasible but also holds potential value in practical applications. The specific conclusions are as follows:

1. As the trajectory of the AUV diverged further from the center of the beacon array and its velocity increased, the errors in the conventional LBL positioning model correspondingly enlarged. The EVLBL positioning model introduced in this study mitigated the positional discrepancies that arose from AUV motion, thereby notably enhancing the accuracy of the localization.

2. Compared with the conventional LS method based on individual beacon data calibration, the proposed overall calibration method for beacon arrays based on the LBL trajectory overlap demonstrated significant advantages in terms of the calibration accuracy and stability. In the simulation experiments, the LS method exhibited large calibration errors for beacons distant from the AUV trajectory (up to 6.40 m). In contrast, the PSO algorithm demonstrated balanced calibration errors across all beacons, with the average error controlled around 3.00 m. This not only enhanced the calibration accuracy but also significantly improved the efficiency of the beacon calibration.

3. When comparing the performances of various algorithms, the EVPSO algorithm exhibited a higher precision in the beacon array calibration, which was attributable to its comprehensive consideration of both the AUV's motion and beacon position errors. The simulation experiments revealed that the calibration errors of the EVPSO algorithm for individual beacons were contained within 1.00 m, marking a notable enhancement in calibration accuracy compared with the PSO, which averaged around 3.00 m.

4. By comparing the RMSE of the LBL system after the beacon array was calibrated using various methods, it became evident that the EVPSO algorithm, with an RMSE of approx-

imately 1.00 m, significantly outperformed both the PSO algorithm (RMSE $\approx$ 1.50 m) and the LS algorithm (RMSE > 5.00 m). This outcome reinforced the validity and precision of the overall calibration method for underwater beacon arrays proposed in this paper, which was based on the EVLBL positioning model.

The EVPSO algorithm proposed in this paper facilitates the calibration of the positions of randomly dispersed underwater acoustic beacon arrays and is compatible with a wide range of underwater unmanned platforms and integrated navigation systems. This is particularly beneficial for time-sensitive tasks, such as underwater archaeology, resource exploration, and underwater rescue operations. Prior to mission execution, the simultaneous deployment of beacons and AUVs can be coordinated in the operational maritime area, facilitated by working vessels or unmanned aerial vehicles. With the assistance of compasses, DVLs, and the randomly positioned beacon array, AUVs can swiftly conduct the calibration of the beacon array. Consequently, this enables the provision of precise navigation services for other underwater equipment.

Although the proposed underwater beacon array calibration method based on EVLBL represents significant progress in enhancing the positioning accuracy and beacon calibration efficiency, there are still some limitations in practical applications. First, this method has extremely strict requirements for time synchronization. In the complex underwater environment, long-term operation often leads to the accumulation of time synchronization errors, which, in turn, has a non-negligible impact on the positioning accuracy. Second, the method proposed in this study was mainly designed and validated for acoustic source beacon arrays, and its applicability to responder beacon arrays remains inadequately verified.

Addressing the aforementioned limitations, future work will focus on several aspects for further research and improvement. Efforts will be made to optimize time synchronization algorithms and enhance the clock accuracy of hardware devices, aiming to reduce error accumulation during long-term operations and consequently improve the positioning accuracy and stability. Second, the scope of application of the method proposed in this paper will be expanded, especially for transponder beacon arrays. Through a thorough analysis of the signal characteristics of transponders, more effective calibration and positioning strategies can be developed to further the utilization of underwater positioning technology in diverse fields.

Author Contributions: Conceptualization, G.Z.; funding acquisition, Z.W.; investigation, G.Z.; methodology, G.Z.; project administration, G.Y.; resources, G.Y. and Y.X.; software, G.Z.; validation, G.Z.; writing—original draft, G.Z.; writing—review and editing, G.Y., Z.W., Y.X. and Z.Q. All authors read and agreed to the published version of this manuscript.

Institutional Review Board Statement: Not applicable.

Informed Consent Statement: Not applicable.

Data Availability Statement: Data are contained within the article.

Conflicts of Interest: The authors declare no conflicts of interest.

References

1. Aiello, G. Marine Geological Studies of the Bay of Naples (Southern Tyrrhenian Sea, Italy): Revised Applications of the Seismo-Stratigraphic Concepts and Evolving Technologies to a Late Quaternary Volcanic Area. *J. Mar. Sci. Eng.* **2024**, *12*, 416. [CrossRef]
2. Su, P.; Lin, L.; Lv, Y.; Liang, J.; Sun, Y.; Zhang, W.; He, H.; Yan, B.; Ji, Z.; Wang, L.; et al. Potential and distribution of natural gas hydrate resources in the South China Sea. *J. Mar. Sci. Eng.* **2022**, *10*, 1364. [CrossRef]
3. Wang, M.; Pang, S.; Jin, K.; Liang, X.; Wang, H.; Yi, H. Construction and experimental verification research of a magnetic detection system for submarine pipelines based on a two-part towed platform. *J. Ocean. Eng. Sci.* **2023**, *8*, 169–180. [CrossRef]
4. Li, Y.; Zhang, X.; Shen, Z. YOLO-Submarine Cable: An improved YOLO-V3 network for object detection on submarine cable images. *J. Mar. Sci. Eng.* **2022**, *10*, 1143. [CrossRef]

5. Pham, D.A.; Han, S.H. Design of combined neural network and fuzzy logic controller for marine rescue drone trajectory-tracking. *J. Mar. Sci. Eng.* **2022**, *10*, 1716. [CrossRef]
6. Paull, L.; Saeedi, S.; Seto, M.; Li, H. AUV navigation and localization: A review. *IEEE J. Ocean. Eng.* **2013**, *39*, 131–149. [CrossRef]
7. Zhang, G.; Yi, G.; Xie, Y.; Wang, S.; Wei, Z. Calibration method of DVL based on position observation information. *Measurement* **2024**, *226*, 113819. [CrossRef]
8. Zhang, T.; Shi, H.; Chen, L.; Li, Y.; Tong, J. AUV positioning method based on tightly coupled SINS/LBL for underwater acoustic multipath propagation. *Sensors* **2016**, *16*, 357. [CrossRef] [PubMed]
9. Yu, X.; Qin, H.D.; Zhu, Z.B. Underwater Localization of AUVs in Motion Using Two-way Travel Time Measurements With Unknown Sound Velocity. *IEEE Trans. Veh. Technol.* **2023**, *72*, 11358–11373. [CrossRef]
10. Cao, J.; Zheng, C.; Sun, D.; Zhang, D. Travel time processing for LBL positioning system. In Proceedings of the 2016 IEEE/OES China Ocean Acoustics (COA), Harbin, China, 9–11 January 2016; IEEE: Piscataway, NJ, USA, 2019; pp. 1–5.
11. Wang, C.; Du, P.; Wang, Z.; Wang, Z. An Underwater Acoustic Network Positioning Method Based on Spatial-Temporal Self-Calibration. *Sensors* **2022**, *22*, 5571. [CrossRef] [PubMed]
12. Zhang, S.; Guo, J.; Hou, H. Calibration Algorithm of Underwater Navigation System Based on Multi-orthogonal Signals. In Proceedings of the 2018 International Conference on Image and Graphics Processing, Hong Kong, China, 24–26 February 2018; pp. 176–179.
13. Zhang, L.; Zhang, T. A robust calibration method for the underwater transponder position based on Gauss-Newton iteration algorithm. In Proceedings of the 2019 7th International Conference on Control, Mechatronics and Automation (ICCMA), Delft, The Netherlands, 6–8 November 2019; IEEE: Piscataway, NJ, USA, 2019; pp. 448–453.
14. Zhang, T.; Zhang, L.; Shin, H.S. A novel and robust calibration method for the underwater transponder position. *IEEE Trans. Instrum. Meas.* **2020**, *70*, 9500512. [CrossRef]
15. Tomczak, A.; Stępień, G.; Abramowski, T.; Bejger, A. Subsea wellhead spud-in marking and as-built position estimation method based on ultra-short baseline acoustic positioning. *Measurement* **2022**, *195*, 111155. [CrossRef]
16. Yao, Y.; Xu, X.; Yang, D.; Xu, X. An IMM-UKF aided SINS/USBL calibration solution for underwater vehicles. *IEEE Trans. Veh. Technol.* **2020**, *69*, 3740–3747. [CrossRef]
17. Da-xiong, J.; Yi-ping, L.; Liu, J. Seafloor transponder calibration using improved perpendiculars intersection. *Appl. Ocean. Res.* **2010**, *32*, 261–266.
18. Zhang, J.; Han, Y.; Zheng, C.; Sun, D. Underwater target localization using long baseline positioning system. *Appl. Acoust.* **2016**, *111*, 129–134. [CrossRef]
19. Zhang, H.; Xu, X. A Local Area Segmentation Algorithm for the Underwater Transponder Calibration. In Proceedings of the 2022 7th International Conference on Robotics and Automation Engineering (ICRAE), Singapore, 18–20 November 2022; IEEE: Piscataway, NJ, USA, 2019; pp. 345–349.
20. Zhang, H.; Xu, X.; Zhang, T.; Wang, D.; Zhou, S.; Zhong, M. Improved Salp Swarm Algorithm for the Calibration of the Underwater Transponder. *IEEE Trans. Instrum. Meas.* **2023**, *72*, 8503310. [CrossRef]
21. Yan, Z.; Deng, C.; Li, B.; Zhou, J. Novel particle swarm optimization and its application in calibrating the underwater transponder coordinates. *Math. Probl. Eng.* **2014**, *2014*, 672412. [CrossRef]
22. Li, D.; Ji, D.; Lin, Y.; Liu, J. Mechanism analysis on large calibration errors of seabottom beacon how to improve navigation peformace. In Proceedings of the 2016 Sixth International Conference on Information Science and Technology (ICIST), Dalian, China, 6–8 May 2016; IEEE: Piscataway, NJ, USA, 2019; pp. 157–162.
23. Wang, Y.; Xu, C.; Xu, H.; Zhao, H.; Liu, J. An integrated navigation algorithm for AUV based on pseudo-range measurements and error estimation. In Proceedings of the 2016 IEEE International Conference on Robotics and Biomimetics (ROBIO), Qingdao, China, 3–7 December 2016; IEEE: Piscataway, NJ, USA, 2019; pp. 1625–1630.
24. Real, M.; Vial, P.; Palomeras, N.; Carreras, M. Underwater Acoustic Localization using pose-graph SLAM. In Proceedings of the OCEANS 2023-Limerick, Limerick, Ireland, 5–8 June 2023; IEEE: Piscataway, NJ, USA, 2019; pp. 1–6.
25. Zhang, T.; Wang, Z.; Li, Y.; Tong, J. A passive acoustic positioning algorithm based on virtual long baseline matrix window. *J. Navig.* **2019**, *72*, 193–206. [CrossRef]